Improved Graphitic Structure of Continuous Carbon Nanofibers via Graphene Oxide Templating

*Dimitry Papkov, Alexander Goponenko, Owen C. Compton, Zhi An, Alexander Moravsky, Xing-Zhong Li, SonBinh T. Nguyen, and Yuris A. Dzenis**

Continuous carbon nanofibers (CNF) present an attractive building block for a variety of multifunctional materials and devices. However, the carbonization of poly(acrylonitrile) (PAN) precursors usually results in CNFs with poor graphitic structure and, consequently, modest/non-optimized properties. This paper reports that the graphitic structure of CNFs can be improved with an addition of a small amount of graphene oxide into PAN prior to processing. Continuous CNFs with 1.4 wt% of graphene oxide nanoparticles are prepared from PAN solutions by electrospinning, stabilized, and carbonized at 800 °C, 1200 °C, and 1850 °C. While the as-prepared graphene oxide-filled PAN nanofibers exhibit a considerable reduction in polymer crystallinity, Raman analysis of the carbonized nanofibers shows that both templating with graphene oxide and increasing the carbonization temperature significantly improve the graphitic order in CNFs. The effect of graphene oxide is more significant at higher carbonization temperatures. Selected area electron diffraction analysis of individual nanofibers reveals increased graphitic order and preferred orientation both in the vicinity of visible graphene oxide nanoparticles and in the regions where nanoparticles were not visible. These results indicate a possibility of global templating in CNFs, where the addition of a small amount of graphene oxide nanoparticles can template the formation of good, preferentially oriented graphitic crystallites in CNFs, leading to improved structure and mechanical and transport properties.

1. Introduction

Carbon nanofibers (CNFs) have enjoyed increasing use in a broad variety of nanotechnology applications, including materials and devices for the energy, environmental, biomedical, electronics, and structural sectors.[1–7] Continuous carbon nanofibers are typically produced by carbonizing electrospun polymer-based precursors.[7,8] In the production of such continuous polymer nanofilaments, dilute polymer solutions are jetted in high electric fields,[8,9] where intensive electrical forces, coupled with electrohydrodynamic instabilities, yield ultrathin nanofibers whose diameters can range from single nanometers to micrometers. This top-down electrospinning process typically produces random nanofiber mats but methods for aligning nanofibers have also been developed.[8,9] The continuous nature of electrospun nanofibers, which facilitates handling and processing while significantly reducing health concerns, distinguishes them from other nanomaterials produced by bottom-up synthetic methods.

CNFs can be produced from a variety of polymers.[7] The most common is poly(acrylonitrile) (PAN),[10] which has been used in the manufacturing of most commercial high-performance carbon fibers due to its high carbon yield and the superior strength of the resulting fibers.[11–13] The manufacturing of CNFs from electrospun PAN precursors usually follows a commercial carbon fiber manufacturing process, which includes oxidative stabilization and carbonization steps;[7,10] however, most continuous CNFs produced to date have exhibited relatively poor graphitic structures. To achieve materials with higher elastic moduli and thermal and electrical conductivities, improved graphitic order is needed. A degree of graphitic order and, particularly, preferential axial orientation of the graphitic nanocrystallites within the fibers is also required for higher carbon fiber strength.

One known way to improve the graphitic structure within a carbon fiber is to increase the carbonization temperature: high-temperature graphitization significantly increases the size and alignment of turbostratic graphitic crystallites in PAN-based carbon fibers,[11–13] resulting in improvements in modulus and

D. Papkov, Dr. A. Goponenko, Prof. Y. A. Dzenis
Department of Mechanical and Materials Engineering
Nebraska Center for Materials and Nanoscience
University of Nebraska-Lincoln
Lincoln, NE 68588-0526, USA
E-mail: ydzenis@unl.edu
Dr. O. C. Compton,[+] Z. An, Prof. S. T. Nguyen
Department of Chemistry
Northwestern University
Evanston, IL 60208, USA
Dr. A. Moravsky
MER Corporation, 7960 South Kolb Road
Tucson, AZ 85706, USA
Dr. X.-Z. Li
Nebraska Center for Materials and Nanoscience
University of Nebraska
Lincoln, NE 68588, USA
[+]Present address: E. I. DuPont de Nemours and Company, Inc., Central Research & Development, Experimental Station, Wilmington, DE 19880, USA

DOI: 10.1002/adfm.201300653

conductivity. While turbostratic ordering of up to 40 graphitic layers has been observed after heat treatment of electrospun CNFs at 3000 °C,[14] fiber processing at such a high temperature requires specialized, expensive equipment. Thus, the ability to improve the quality and ordering of the graphitic structures in CNFs at lower carbonization temperatures is highly desirable for economic manufacturing and applications.

An alternative strategy for improving the quality and ordering of the graphitic structures within a carbon fiber is to increase the alignment of the polymer chains inside the polymer precursor fiber. Such increased alignment has been found to improve the elastic modulus of the PAN precursor fibers, which directly correlated to the modulus of the final carbon fibers.[15] The alignment of polymer chains inside the polymer precursor fibers can be improved by, among other methods, incorporating oriented inclusions that possess high surface area and can interact strongly with polymer chains to pre-organize them in a manner that maximizes chain orientation. Carbon-based nanoinclusions that possess long range, ordered graphitic structure would be especially beneficial as they can both organize the polymer chains and simultaneously serve as a "templating" agent for the formation of graphitic crystallites during carbonization.

Carbon nanotubes (CNT) have been used as a nanoscale reinforcement and templating agent in several types of fibers. Single-walled carbon nanotubes (SWNT) were found to improve crystallization and chain orientation in polypropylene fibers.[16] Incorporation of CNTs into gel-spun PAN-based carbon microfibers has been shown to result in improved graphitic order and mechanical properties.[17] CNTs have also been integrated into electrospun polymer nanofibers,[18,19] and were shown to increase polymer chain alignment in PAN nanofibers.[19] Composite CNT/polymer nanofibers have been successfully converted into CNFs[20–23] and high-resolution transmission electron microscopy (HRTEM) analysis confirmed an improved local graphitic structure of CNFs in the vicinity of the CNTs.[24,25] However, improvements in structure and mechanical properties reported to date have been modest. In addition, manufacturing of CNT-reinforced nanofibers has been challenging and the quality of the resulting CNFs is generally poor. For example, CNTs are often curved, causing grown graphitic layers to follow the curvature.[22,25] Other artifacts, such as CNT ends "sticking out" of the CNFs and other imperfections, have also been reported or can be distinguished in the provided images.[18,19,21,22]

Recently, graphene and graphene oxide have attracted high interest as new types of nanoscale carbon.[26] Fully exfoliated and stable graphene and graphene oxide nanoparticles can now be produced very inexpensively by several methods.[26] In addition to having properties that rival those of carbon nanotubes, graphene and graphene oxide have large surface areas that can interact strongly with a wide range of polymers.[27–32] Recent studies have demonstrated that the addition of low volume fractions of graphene-based nanoparticles to polymers led to property improvements exceeding those observed for SWNTs or any other form of carbon at comparable particle loadings.[28,31] Notably, a dramatic 40 °C increase in the glass transition temperature (T_g) of PAN was recorded with only 1 wt% of functionalized graphene inclusions.[28] Such a large effect indicates strong polymer–graphene interaction that is promising for pre-organizing polymer chains into aligned structures that can readily form oriented graphitic crystallites during the carbonization of the polymer nanofibers. Surprisingly, graphene-based nanoparticles have not yet been used as templating agents in carbon fibers or nanofibers, to the best of our knowledge. Herein, we introduce graphene oxide as an orienting and templating agent in PAN-based carbon nanofibers. We show that incorporation of a small amount of graphene oxide significantly improved graphitic order and orientation in continuous CNFs upon carbonization at relatively low temperatures.

2. Results and Discussion

2.1. Fabrication and Characterization of PAN-based Precursor Nanofibers

The small graphene oxide nanoparticles that we employed in our work were obtained by subjecting SP-1 graphite-derived graphene oxide to high-power ultrasonication (see Supporting Information for synthetic procedures and characterization details). The particle size distribution of this material in dispersion, as measured by dynamic light scattering (DLS), can be seen in **Figure 1**a (it should be noted that dynamic light scattering measurements model particles as spheres, which is not

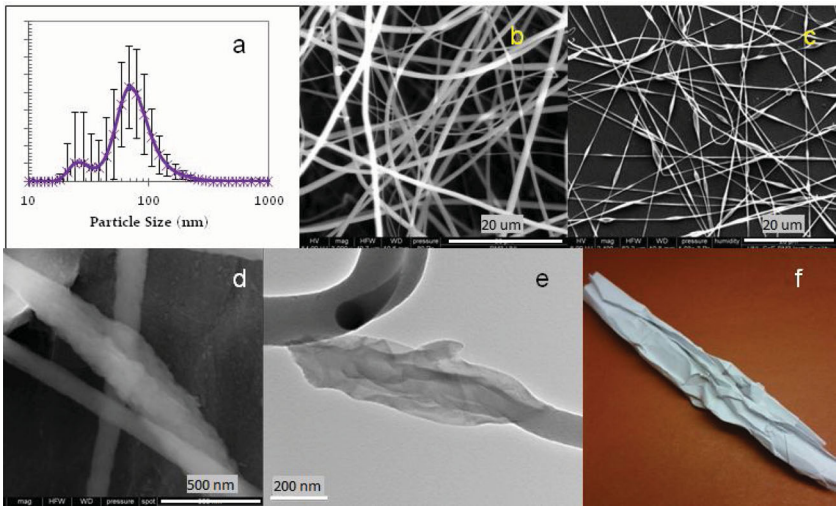

Figure 1. Graphene oxide nanoparticles and electrospun nanofibers: a) DLS size-distribution plot of the graphene oxide nanoparticles; b) a scanning electron microscopy (SEM) image of electrospun pristine PAN nanofibers; c) an SEM image of graphene oxide-templated PAN nanofibers; d) an SEM image of a thicker area of as-spun templated PAN nanofiber showing wrinkled structure with crumpled graphene oxide particle; e) a TEM image of a thicker area in carbonized templated nanofiber; f) a paper model of a graphene oxide sheet anisotropically crumpled by radial forces inside the nanofiber during electrospinning.

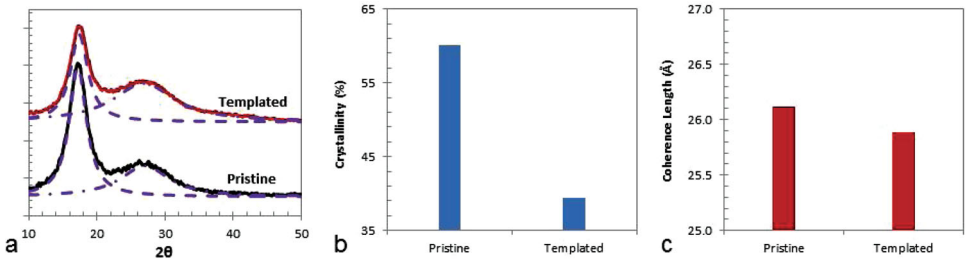

Figure 2. XRD analysis of as-spun nanofibers: a) XRD diffractograms of pristine and graphene oxide-templated PAN NFs (the dashed lines represent the fitted peaks), b) crystallinity, and c) coherence length of PAN structure obtained from XRD analysis of pristine and graphene oxide-templated samples.

true for graphene oxide sheets, and hence the particle size in the charts should not be taken as the true particle size). The DLS scans show broad bimodal size distribution and indicate presence of relatively large particles (>100 nm), which may affect the morphology of the electrospun nanofibers even though the average size of the particle sample is small.

Nanofibers containing ≈1.4 wt% graphene oxide were produced by electrospinning. More information on nanomanufacturing can be found in the Experimental Section and in the Supporting Information. Assuming that PAN would undergo a larger weight loss than graphene oxide during oxidation and carbonization, the weight fraction of graphene oxide in the carbonized nanofibers would be slightly higher than this value; however, the exact relative weight losses could not be measured. Both PAN-based precursor and carbon nanofibers containing graphene oxide will be referred to as graphene oxide-"templated" nanofibers for simplicity. As controls, we also examined pristine PAN precursor nanofibers (from a 10 wt% solution of PAN in DMF) and the CNFs derived from them, produced under conditions similar to those for the corresponding graphene oxide-templated materials.

Figures 1b,c present the overall morphology of as-spun pristine and graphene oxide templated nanofibers (NF). The NFs containing graphene oxide were slightly thinner than the pristine NFs but exhibited occasional thicker regions that appeared to contain larger graphene oxide particles. Closer examination of these regions (Figure 1d) revealed the presence of crumpled graphene oxide particles inside the PAN matrix. Such crumpling is not unusual for exfoliated graphene sheets that have been shown to bend and fold easily into various shapes depending on substrate or temperature,[33] and are also capable of rolling spontaneously into scrolls under certain conditions.[34] We note that graphene oxide nanoparticles have been processed into crumpled particles by dispersing them into aerosol droplets whose solvents were then evaporated quickly.[35,36] The crumpling of graphene oxide particles inside our nanofibers (Figure 1) could be caused by similar radial forces in the fast-thinning electrospun jets. Nevertheless, these particles were all still covered by PAN. The nanofiber regions with no visible graphene oxide particles had uniform diameters with relatively little variation between the different fibers (Figure 1c), as opposed to a broader distribution of diameters and generally thicker nanofibers in the case of pristine NFs (Figure 1b). Smaller diameters of the templated NFs were most likely due to higher conductivity of the polymer solution containing graphene oxide.

As-spun PAN nanofibers were analyzed by wide-angle X-ray diffraction (WAXD). The resulting X-ray diffractograms (**Figure 2**a) exhibited a crystalline peak at 2θ ≈17.4° (corresponding to d-spacing of ≈5.1 Å) and a broad amorphous halo at approximately $2\theta \approx 26.9°$, typical of semicrystalline PAN.[37] The XRD-derived crystallinity and coherence length were extracted as described in the Experimental Section and are shown in Figure 2b,c. While the average coherence length remained relatively unchanged in the two types of nanofibers, the XRD-derived crystallinity of PAN was found to decrease significantly (by ≈33%) in the presence of graphene oxide nanoparticles.

The significant reduction of PAN crystallinity in the presence of graphene oxide is in contrast to the effects usually reported for CNT-filled polymers. However, it is consistent with the previously described large increase in PAN T_g,[28] which indicates reduced macromolecular mobility as a result of strong polymer–graphene interaction over extensive interfacial area. We note that the surface area of graphene oxide nanoparticles available for interaction with PAN did not necessarily decrease with crumpling, unless the graphene oxide layers folded upon themselves to form a tight stack. As no such stacks were observed in the electrospun NFs, strong polymer–nanoparticle interaction and reduced chain mobility are likely causes of lower polymer crystallinity.

A survey of the carbon fiber literature suggests that the crystallinity of PAN does not play a major role in the stabilization and carbonization of fibers. In fact, the use of co-monomers in the production of PAN precursors to commercial carbon fibers usually reduces the crystallinity of PAN at the precursor-fiber stage, yet results in carbon fibers with better structure and properties.[11–13] However, it is important that the polymer chains within both amorphous and crystalline regions of these precursor fibers are well-aligned along the fiber axis. Note that, unlike the isotropic crumpling produced by evaporation-driven shrinkage of aerosol droplets,[35,36] the crumpling of graphene oxide nanoparticles inside the electrospun nanofibers is anisotropic (Figure 1). The clearly visible axial symmetry is most likely the result of nanoparticle orientation by the shear forces in the electrospun jets (the particle normal is oriented perpendicularly to the jet axis) followed by radial crumpling. In this case, the polymer chains in the vicinity of the crumpled nanoparticles can still maintain, and even further enhance, their

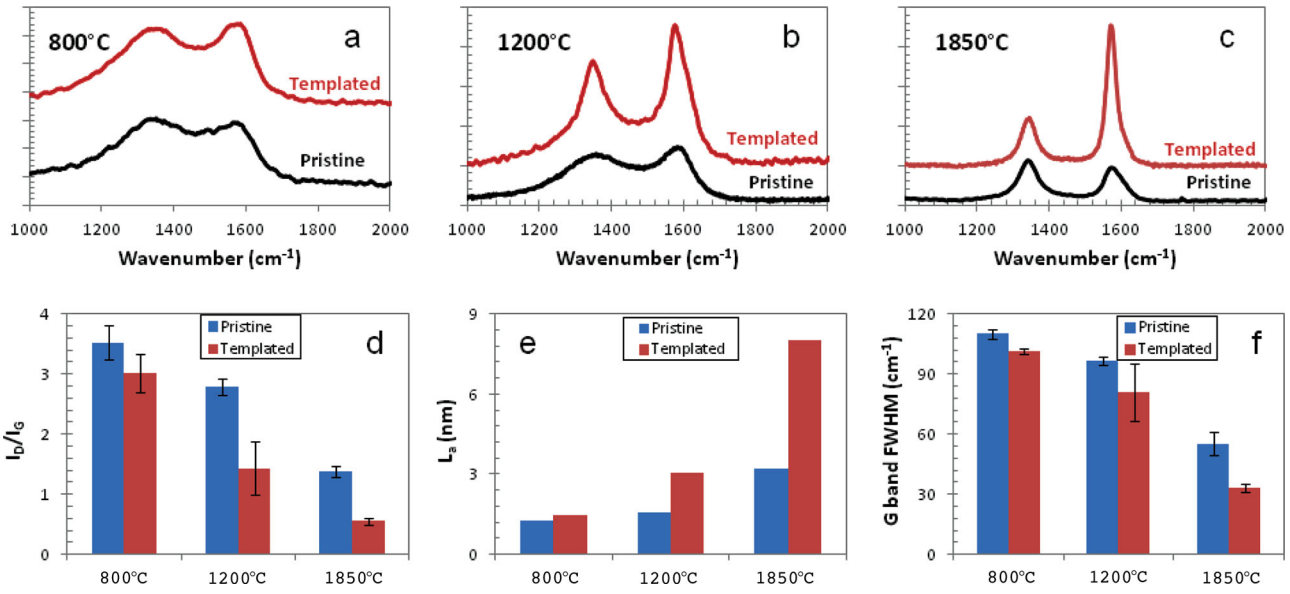

Figure 3. a–c) Raman spectra of carbon nanofibers prepared from pristine PAN and graphene oxide-templated samples that have been carbonized at a) 800 °C, b) 1200 °C, and c) 1850 °C. d) I_D/I_G ratios for the two sets of samples at different carbonization temperatures. e) Calculated L_a values for the two sets of samples at different carbonization temperatures. f) FWHM values of the G band for the two sets of samples at different carbonization temperatures.

preferred alignment along the fiber axis. Simultaneously, their reduced mobility can help preserve this alignment during stabilization and carbonization.

2.2. Fabrication and Characterization of Carbon Nanofibers

Mats of the PAN-based precursor nanofibers were stabilized in air at 270 °C and carbonized under nitrogen atmosphere at 800 °C, 1200 °C, or under vacuum at 1850 °C, with a heating rate of 10 degrees per minute and dwell time of one hour. TEM analysis of the post-carbonization graphene oxide-templated CNFs (Figure 1e) revealed that the anisotropic crumpled morphology of the graphene oxide nanoparticle was preserved during carbonization. Selected area electron diffraction (SAED) from the same spot did not show any 3D crystalline order, confirming full graphene oxide exfoliation and random nature of radial nanoparticle crumpling, as opposed to possible more regular folding or scrolling. The anisotropic, statistically axisymmetric nature of crumpling is clearly visible in the TEM image shown in Figure 1e.

The Raman spectra of pristine and templated CNFs carbonized at different temperatures (**Figure 3**a–c) show significant differences between the two materials, as indicated by the extracted parameters shown in Figures 3d–f. The integrated intensities I_D and I_G and the width of the G band were calculated by fitting the D and G peaks using Lorentzian curve shapes. The ratio $R = I_D/I_G$ was originally linked by Tuinstra and Koenig[38] to the in-plane crystallite size L_a (R proportional to L_a^{-1}) and was subsequently widely used for this purpose,[20,24,39–42] although there have been reports of this relationship breaking down for crystals smaller than 2 nm.[43,44] The width of the G band is also often used as an indicator of the level of graphitization (narrower G band indicates better graphitic structure). The templated CNFs showed improved graphitic structure as indicated by smaller R, larger L_a, and smaller FWHM (full-width half maximum) of the G band (see Figure 3d–f). The graphitic structure significantly improved for both groups of samples at higher carbonization temperatures, with the templated samples showing greater improvements. Together with the aforementioned XRD analysis of the templated precursor nanofibers, these results clearly suggest that the significant improvements in the graphitic structure of the resulting CNFs were a direct consequence of the addition of a small amount of graphene oxide nanoparticles into the PAN nanofibers. We note that because both XRD and Raman analyses are not localized techniques, the information that they provide is an average of data for nanofiber bundles containing multiple nanofilaments.

2.3. SAED Analysis of Carbon Nanofibers

The structure of pristine and graphene oxide-templated nanofibers carbonized at different temperatures was also examined by SAED. For the latter set of samples, data were collected from nanofiber regions containing visible, larger graphene oxide nanoparticles as well as from more-uniform nanofiber regions without visible nanoparticles. Typical two-dimensional SAED patterns are shown in **Figure 4**a, along with the corresponding digital intensity profiles (Figures 4b–d). Analysis of these data further confirms that templating led to significant improvements in graphitic structure of CNFs, as seen in the more-pronounced and sharp (002) and (100) diffraction peaks. The SAED patterns of both regions (those with visible graphene oxide particles and those where no such particles were observed) of the templated samples were qualitatively similar over all carbonization temperatures, indicating the global

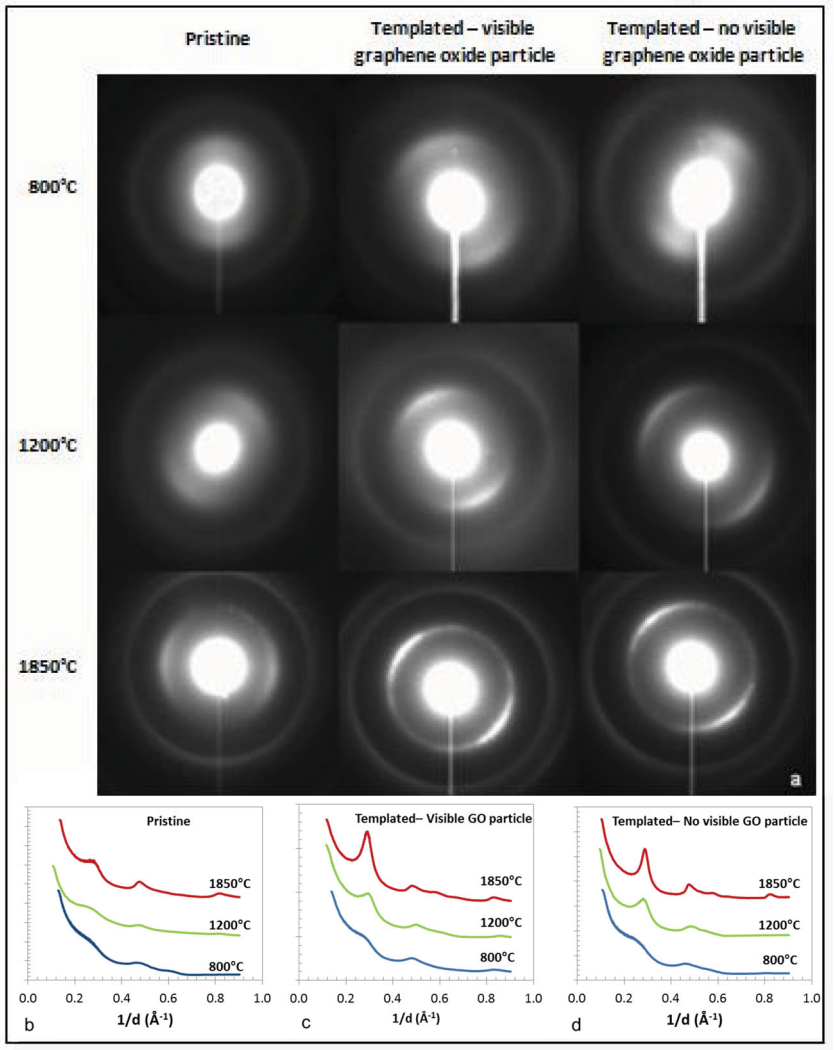

Figure 4. Electron diffraction analysis of carbon nanofibers. a) Typical 2D SAED patterns for pristine and graphene oxide-templated CNFs (in regions with and without visible graphene oxide particles) at different carbonization temperatures. b–d) Digital intensity profiles for b) pristine sample, c) graphene oxide-templated sample in the region with visible graphene oxide particles, and d) graphene oxide-templated sample in the region with no visible graphene oxide particles.

In addition to size and quality, the orientation of graphitic nanocrystals with respect to the CNF fiber axis is a significant parameter governing the mechanical and transport properties of carbon fibers. Crystal orientation was examined in pristine and templated nanofibers carbonized at 800 °C and 1850 °C. The arc double angles for the (002) reflections (estimated as FWHM; see **Figure 5**a,b) were obtained using the QPCED2 program[45] from the calculated azimuthal variations of the (002) reflections. As before, data were evaluated for regions with and without visible graphene oxide nanoparticles in templated CNFs (Figure 5c,d). The average FWHM values and the corresponding 95% confidence intervals shown in Figure 5e were computed based on the analysis of 5–20 scans for each specimen type.

Analysis of the SAED data in Figure 5 suggests that all CNF specimens exhibited preferred orientation of the (002) planes parallel to the fiber axis. However, the degree of this preferred orientation, as expressed by the (002) arc double angle, was higher in the templated CNFs. A two-parameter factorial analysis of the (002) double angles[46] showed no statistically significant difference (at α = 0.05 confidence level) between the orientation in thicker regions of the templated CNFs (the regions with visible graphene oxide nanoparticles) and the thinner ones (without visible graphene oxide nanoparticles), again consistent with a global templating scenario. The graphitic nanocrystals in both regions in the graphene oxide-templated CNFs were more preferentially oriented along the fiber axis than those in the pristine CNFs. Interestingly, this preferred orientation was roughly independent of the carbonization temperature.

nature of the templating effect. For pristine samples, the level of improvement in graphitic structure with the increase of carbonization temperature was moderate: the diffraction patterns for samples carbonized at 1200 °C were quite similar to those for samples carbonized at 800 °C; it is only with the 1850 °C carbonization temperature that a marked improvement can be seen (compare the panels in the left column of Figure 4a). In contrast, the templated samples showed significant improvement for the 1200 °C carbonization temperature and remarkable improvement for the 1850 °C carbonization. These results are consistent with the Raman data discussed earlier. We note that both 1200 °C and 1850 °C carbonization temperatures in this study are relatively low compared to typical temperatures used to achieve high quality graphitic structures that are in the range from 2500–3000 °C.

2.4. Discussion of Possible Mechanisms of Improvements

Not only do the aforementioned results show apparent global improvements in the quality of the graphitic structure and its preferred orientation in PAN-derived CNFs as a result of a small addition of graphene oxide templating nanoparticles, they also indicate an apparent acceleration of the graphitization process in the presence of graphene oxide at intermediate carbonization temperatures. These effects can be the result of axial propagation of the templated graphitic order nucleated by the larger, visible graphene oxide nanoparticles. Alternatively, the good graphitic structure of the thinner, uniform regions of the templated CNFs and the apparent global nature of improvements can be attributed to the presence of smaller graphene oxide nanoparticles in these regions. Although there is no definitive evidence at

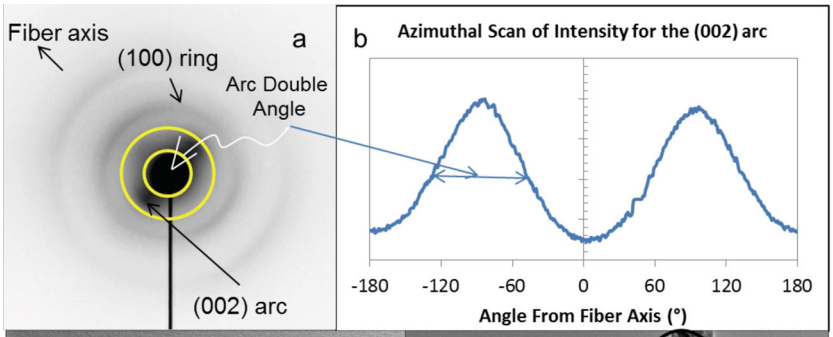

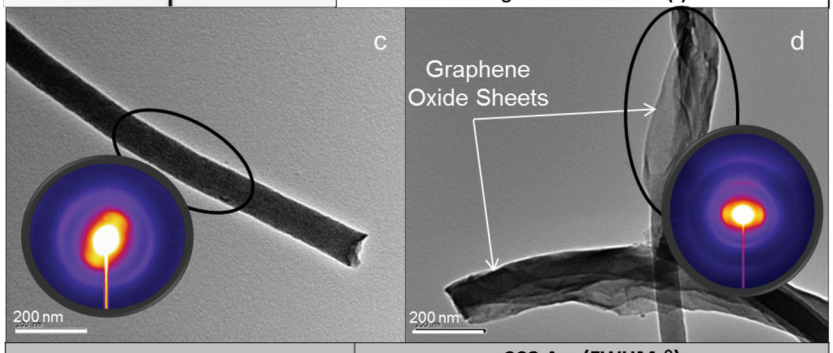

e Sample	002 Arc (FWHM °)	
	800°C	1850°C
PAN	84±3.3	77±4.8
Templated – visible particle	61±6.6	64±6.0
Templated – no visible particle	65±6.0	64±5.6

Figure 5. Electron diffraction analysis of orientation in carbon nanofibers. a) Example 2D SAED pattern for pristine CNF carbonized at 800 °C showing (100) ring and (002) arc with reference to fiber axis orientation. b) Computed azimuthal variations of the (002) scattering intensities integrated between the two yellow concentric rings. c) TEM image and SAED diffraction from carbonized graphene oxide-templated nanofiber in the area without visible graphene oxide particles. d) TEM image and SAED diffraction from carbonized graphene oxide-templated nanofiber in the area with visible graphene oxide particles (in both cases SAED was enhanced for visual purposes only). e) Comparison of (002) arc double angles for carbonized pristine and graphene oxide-templated samples in the areas with and without visible graphene oxide particles (the ± values represent 95% confidence intervals).

this time, we believe that the latter smaller nanoparticles play an important role as they are the primary particles present in the nanofibers (the DLS particle size distribution in Figure 1a shows that graphene oxide particles larger than 100 nm represent just the tail of the broad distribution). As the electrospun jets thin down, these smaller particles are likely to experience similar orientation and crumpling forces, resulting in multiple radially crumpled smaller nanoparticles distributed within the CNFs (the crumpling process is complex and depends on the peculiarities of inhomogeneous solvent evaporation and flow profiles in electrospun jets;[47] however, that should not affect the overall crumpling tendency and axial symmetry). These distributed nanoparticles may then be responsible for the observed near-uniform CNF templating evidenced by SAED. Together, our XRD, Raman, and SAED data clearly indicate that the global templating of graphitic structures in electrospun nanofibers is possible with a small quantity of graphene oxide nanoparticles. This observation is consistent with large changes in structure and properties of graphene nanocomposites observed at very low graphene contents.[27–32]

In conventional carbon fibers, improved graphitic structure and orientation are believed to be closely related to improved alignment of the polymer chains in PAN-based precursor fibers,[15,48,49] which consist of oriented ordered (crystalline) and disordered (amorphous) regions.[48] Because the alignment in amorphous regions can easily relax upon heating, before the carbonization begins, the fiber must be constrained if good graphitic structure and orientation are to be achieved.[48,49] Indeed, the discovery that constraining precursor fiber during stabilization can improve carbon fiber properties[50] is now widely regarded as the key to high-performance carbon fibers.[49] This constraint prevents fast entropic shrinkage and loss of orientation in the non-crystalline regions of PAN fibers and results in better structure and orientation and reduced probability of defect formation in carbon fibers.

Interestingly, the structure and preferred orientation of the graphitic nanocrystals in our graphene oxide-templated CNFs were significantly improved in spite of the observed increase in the amorphous phase content and the lack of constraint during stabilization and carbonization of the precursor nanofibers. (Recall that XRD analysis of templated PAN nanofibers showed significant crystallinity reduction; the crystallization of PAN was most likely disrupted by strong polymer interaction with the irregularly shaped, crumpled graphene oxide particles.) We speculate that "anchoring" (i.e., attachment via strong interaction) of polymer chains on the surface of graphene oxide nanoparticles could play a role similar to the traditional mechanical constraint (usually applied through stretching). This anchoring may prevent polymer shrinkage and loss of alignment at the beginning of the stabilization process. The irregular crumpled shape of the graphene oxide template might further help the anchoring via mechanical interlocking.

It is interesting to note that, in addition to the possible beneficial role that graphene oxide plays in polymer chain anchoring, the irregular shape of the radially crumpled sheets closely matches the popular model of the high-strength carbon fiber structure,[13,51] which consists of irregular, longitudinally wrinkled turbostratic graphitic stacks with preferred axial orientation. A special agitation method during fiber spinning was developed to achieve this preferred randomized folded turbostratic structure due to its beneficial effects on properties.[52] In this sense, the oriented crumpled graphene oxide particle geometry seen in Figure 1 may represent a useful natural template to achieve a similar high-strength carbon fiber structure in either conventional microfibers or electrospun continuous nanofibers under simplified, more economic manufacturing protocols. In addition, the crumpled graphene oxide particles

may provide multiple nucleation sites for graphitic crystal growth during carbonization, especially because the carbon atoms along the crumpled folds are more reactive.[53,54]

The use of nanocarbon templating may also open up an intriguing possibility of improving graphitic order and preferred orientation in carbon fibers without increasing the amount and size of voids. During carbonization at high temperatures, larger voids in carbon fibers can form as growing ordered graphitic regions "consume" their neighboring disordered regions.[52,55] These voids are detrimental to fiber strength and perhaps are the main reason for the classical modulus-strength trade-off in highly graphitic carbon fibers. Void formation in the nanocarbon-templated micro- and nanofibers can be reduced as the graphitic structure evolution progresses via continuous growth in the direction perpendicular to the nanoparticle surface. Other void-formation mechanisms, such as inadequate oxygen diffusion or entrapment of gaseous products during stabilization and carbonization of conventional microfibers, will be further alleviated in CNFs due to ultra-small nanofiber diameters. Better graphitic structure and orientation with fewer voids should then lead to simultaneous improvements in modulus, transport properties, and strength of carbon NFs.

3. Conclusions

The incorporation of a very small amount of graphene oxide nanoparticles into PAN matrix was shown to have several beneficial effects on the graphitic structure and preferred orientation of the CNFs formed from the resulting composite nanofibers. While our experimental results indicate that the templating occurs "globally" throughout the whole fiber structure, more studies are needed to further understand and manipulate the templating effect as a function of the weight fraction of the graphene oxide nanoparticles, their size distribution and surface chemistry defining the level of graphene oxide interactions with the PAN chains, and the electrospinning process parameters, which control the nanofiber diameters, the degree of nanoparticle crumpling and orientation, and the polymer chain orientation. If the templating effect can indeed be controlled and tuned, our strategy can provide an inexpensive route to continuous carbon nanofibers with greatly improved structure and properties. The proposed templating methodology should be highly economical as it utilizes inexpensive templating additives, an efficient top-down nanomanufacturing process, and relatively low carbonization temperatures.

4. Experimental Section

Electrospinning of Nanofiber Mats and Subsequent Carbonization: Nanofibers were electrospun from a (10/0.14 wt%/wt%) dispersion of PAN/graphene oxide in dimethylformamide (DMF) at 12 KV over a 20 cm spinneret-collector distance, using a 0.6 mL h^{-1} feed rate and a 20 gauge needle. Mats of the PAN-based precursor nanofibers were stabilized in air at 270 °C and carbonized at three different temperatures: under nitrogen atmosphere at 800 °C and 1200 °C, or under vacuum at 1850 °C, with a heating rate of 10° min^{-1} and dwell time of 1 h in all cases.

X-Ray Diffraction: As-spun nanofibers were analyzed by XRD using a Rigaku Multiflex X-ray diffractometer with Cu Kα radiation in the range of 2θ between 10 and 50 degrees. After removing the background, the crystalline peak and the amorphous halo were fitted using Lorentzian peak shapes. The XRD-derived polymer crystallinity was evaluated by dividing the area under the crystalline peak by the total area under the curve. The coherence length (in Å) was calculated from the width of the main crystalline peak, using the Scherrer equation:

$$\text{C.L.} = \frac{K\lambda}{\beta\cos\theta} = \frac{0.9\times 1.542}{\sqrt{(\text{FWHM}^2 - 0.002^2)}\cos\theta}$$

where shape factor K was taken as 0.9, λ is the standard wavelength for a copper source (in Å), 0.002 is the instrumental peak widening calculated based on a single crystal Si standard, θ is the Bragg angle for the crystalline peak, and the FWHM is measured in rad.

Raman Spectra: Raman spectroscopic analysis was carried out at the University of Nebraska-Lincoln. First-order Raman spectra (1000–2000 cm^{-1}) at 1.67 cm^{-1} step were obtained, using an inVia Raman microscope from Renishaw with a 514 nm laser as an excitation source. D (1335–1350 cm^{-1}) and G (1565–1585 cm^{-1}) bands were fitted using Lorentzian curve shapes, and the integrated intensities I_D and I_G and the width of G bands were calculated. Measurements were performed at five different locations on each fiber mat, from which average and standard deviation values were calculated.

Select Area Electron Diffraction: SAED patterns were collected at the University of Nebraska-Lincoln using a JEM 2010 transmission electron microscope from JEOL. At least 5 CNFs were examined for each type of material, carbonization temperature, and the nanofiber region. Data analysis was carried out using the QPCED2 software,[45] and the digital intensity profiles were computed by a 360° azimuthal integration of the 2D image. The arc double angles were obtained from the calculated azimuthal variations of the (002) reflections.

Supporting Information

Supporting Information is available from the Wiley Online library or from the author.

Acknowledgements

This work was supported in part by the ARO (MURI award No. W911NF-09-1-0541), AFOSR (FA9550-11-1-0204), and NSF (NIRT-0709333, CMMI-0600675, and CBET-1140065). OCC was an NSF ACC fellow (NSF Award CHE-0936924).

Received: February 20, 2013
Revised: April 23, 2013
Published online: June 19, 2013

[1] M. J. Laudenslager, R. H. Scheffler, W. M. Sigmund, *Pure Appl. Chem.* **2010**, *82*, 20.
[2] J. Park, Y. Ju, S. Park, H. Jung, K. Yang, W. Lee, *J. Appl. Electrochem.* **2009**, *39*, 1229.
[3] J. Miao, M. Miyauchi, T. J. Simmons, J. S. Dordick, R. J. Linhardt, *J. Nanosci. Nanotechnol.* **2010**, *10*, 5507.
[4] P. A. Tran, L. Zhang, T. J. Webster, *Adv. Drug Delivery Rev.* **2009**, *61*, 1097.
[5] Y. A. Dzenis, *Science* **2008**, *319*, 419.
[6] T. Chou, L. Gao, E. T. Thostenson, Z. Zhang, J. Byun, *Composites Sci. Technol.* **2010**, *70*, 1.
[7] M. Inagaki, Y. Yang, F. Kang, *Adv. Mater.* **2012**, 2547.
[8] Y. A. Dzenis, *Science* **2004**, *304*, 1917.
[9] A. Greiner, J. H. Wendorff, *Angew. Chem., Int. Ed.* **2007**, *46*, 5670.
[10] Y. A. Dzenis, Y. Wen, in *Continuous Carbon Nanofibers for Nanofiber Composites*, MRS Proceedings, MRS Fall Meeting, Vol. *702*, **2001**.

[11] E. Fitzer, *Carbon* **1989**, *27*, 621.
[12] M. K. Jain, A. S. Abhiraman, *J. Mater. Sci.* **1987**, *22*, 278.
[13] A. K. Gupta, D. K. Paliwal, P. Bajaj, *J. Macromol. Sci., Polym. Rev.* **1991**, *31*, 1.
[14] Z. Kurban, A. Lovell, D. Jenkins, S. Bennington, I. Loader, A. Schober, N. Skipper, *Eur. Polym. J.* **2010**, *46*, 1194.
[15] G. Henrici-Olivé, S. Olivé, *Adv. Polym. Sci.* **1983**, *51*, 1.
[16] A. R. Bhattacharyya, T. V. Sreekumar, T. Liu, S. Kumar, L. M. Ericson, R. H. Hauge, R. E. Smalley, *Polymer* **2003**, *44*, 2373.
[17] H. G. Chae, M. L. Minus, A. Rasheed, S. Kumar, *Polymer* **2007**, *48*, 3781.
[18] R. Sen, B. Zhao, D. Perea, M. E. Itkis, H. Hu, J. Love, E. Bekyarova, R. C. Haddon, *Nano Lett.* **2004**, *4*, 459.
[19] L. Vaisman, E. Wachtel, H. D. Wagner, G. Marom, *Polymer* **2007**, *48*, 6843.
[20] F. Ko, Y. Gogotsi, A. Ali, N. Naguib, H. Ye, G. L. Yang, C. Li, P. Willis, *Adv. Mater.* **2003**, *15*, 1161.
[21] H. Hou, J. J. Ge, J. Zeng, Q. Li, D. H. Reneker, A. Greiner, S. Z. D. Cheng, *Chem. Mater.* **2005**, *17*, 967.
[22] T. Maitra, S. Sharma, A. Srivastava, Y. Cho, M. Madou, A. Sharma, *Carbon* **2012**, *50*, 1753.
[23] I. H. Chen, C. C. Wang, C. Y. Chen, *J. Phys. Chem. C* **2010**, *114*, 13532.
[24] S. Prilutsky, E. Zussman, Y. Cohen, *Nanotechnology* **2008**, *19*, 165603.
[25] S. Prilutsky, E. Zussman, Y. Cohen, *J. Polym. Sci., Part B: Polym. Phys.* **2010**, *48*, 2121.
[26] O. C. Compton, S. T. Nguyen, *Small* **2010**, *6*, 711.
[27] S. Stankovich, D. A. Dikin, G. H. B. Dommett, K. M. Kohlhaas, E. J. Zimney, E. A. Stach, R. D. Piner, S. T. Nguyen, R. S. Ruoff, *Nature* **2006**, *442*, 282.
[28] T. Ramanathan, A. A. Abdala, S. Stankovich, D. A. Dikin, M. Herrera-Alonso, R. D. Piner, D. H. Adamson, H. C. Schniepp, X. Chen, R. S. Ruoff, S. T. Nguyen, I. A. Aksay, R. K. Prud'Homme, L. C. Brinson, *Nat. Nanotechnol.* **2008**, *3*, 327.
[29] M. A. Rafiee, J. Rafiee, I. Srivastava, Z. Wang, H. Song, Z. Yu, N. Koratkar, *Small* **2010**, *6*, 179.
[30] J. R. Potts, D. R. Dreyer, C. W. Bielawski, R. S. Ruoff, *Polymer* **2011**, *52*, 5.
[31] M. A. Rafiee, J. Rafiee, Z. Wang, H. Song, Z. Yu, N. Koratkar, *ACS Nano* **2009**, *3*, 3884.
[32] D. D. Kulkarni, I. Choi, S. S. Singamaneni, V. V. Tsukruk, *ACS Nano* **2010**, *4*, 4667.
[33] Z. Xu, M. J. Buehler, *ACS Nano* **2010**, *4*, 3869.
[34] L. M. Viculis, J. J. Mack, R. B. Kaner, *Science* **2003**, *299*, 1361.
[35] J. Luo, H. D. Jang, T. Sun, L. Xiao, Z. He, A. P. Katsoulidis, M. G. Kanatzidis, J. M. Gibson, J. Huang, *ACS Nano* **2011**, *5*, 8943.
[36] X. Ma, M. R. Zachariah, C. D. Zangmeister, *Nano Lett.* **2012**, *12*, 486.
[37] Z. Bashir, A. R. Tipping, S. P. Church, *Polym. Int.* **1994**, *33*, 9.
[38] F. Tuinstra, J. L. Koenig, *J. Compos. Mater.* **1970**, *4*, 492.
[39] D. S. Knight, W. B. White, *J. Mater. Res.* **1989**, *4*, 385.
[40] S. Reich, C. Thomsen, *Philos. Trans. R. Soc., A* **2004**, *362*, 2271.
[41] L. G. Cancado, K. Takai, T. Enoki, M. Endo, Y. A. Kim, H. Mizusaki, A. Jorio, L. N. Coelho, R. Magalhaes-Paniago, M. A. Pimenta, *Appl. Phys. Lett.* **2006**, *88*, 163106.
[42] J. Rafique, J. Yu, X. Zha, K. Rafique, *Bull. Mater. Sci.* **2010**, *33*, 553.
[43] A. C. Ferrari, J. Robertson, *Phys. Rev. B* **2000**, *61*, 14095.
[44] A. C. Ferrari, *Solid State Commun.* **2007**, *143*, 47.
[45] X. Li, *J. Appl. Crystallogr.* **2012**, *45*, 862.
[46] *SAS Proc Glimmix software Version 9.2 TS* SAS Institute, Inc. **2002–2008**.
[47] X. Wu, Y. Salkovskiy, Y. A. Dzenis, *Appl. Phys. Lett.* **2011**, *98*, 223108.
[48] M. K. Jain, M. Balasubramanian, P. Desai, A. S. Abhiraman, *J. Mater. Sci.* **1987**, *22*, 301.
[49] S. Damodaran, P. Desai, A. S. Abhiraman, *J. Text. Inst.* **1990**, *81*, 384.
[50] W. Watt, L. N. Phillips, W. Johnson, *The Engineer* **1966**, *221*, 815.
[51] S. C. Bennet, D. J. Johnson, in *Proc. 5th London Carbon and Graphite Conf.*, Vol. *1*, Society of Chemical Industry, London, **1978**.
[52] X. Huang, *Materials* **2009**, *2*, 2369.
[53] R. Ruoff, *Nature* **2012**, *483*, S42.
[54] D. Srivastava, D. W. Brenner, J. D. Schall, K. D. Ausman, M. Yu, R. S. Ruoff, *J. Phys. Chem. B* **1999**, *103*, 4330.
[55] C. N. Tyson, *J. Phys. D* **1975**, *8*, 749.